Confinement of Symmetric Diblock Copolymer Thin Films

Wilfred H. Tang[†]

Department of Chemistry and The James Franck Institute, University of Chicago, Chicago, Illinois 60637

Received June 18, 1999; Revised Manuscript Received October 4, 1999

ABSTRACT: We study symmetric and nearly symmetric diblock copolymers confined to thin films of thickness L, where L is the equilibrium bulk lamellar period. The film surfaces have opposite preferences for the polymer species; this results in frustration. We use the Scheutjens−Fleer method to calculate the free energies of several parallel (with respect to the film surfaces), perpendicular, and mixed perpendicular morphologies as a function of the preferential wetting strengths of the polymer species at the film surfaces. When the film surface is highly preferential, the perpendicular morphology adopts a novel structure not seen in bulk diblock copolymer melts. In addition, when the diblock copolymers are slightly asymmetric, a mixed perpendicular morphology, in which half of the film resembles the perpendicular morphology and half of the film resembles a parallel morphology, can be stable. We calculate a phase diagram in the plane of the preferential wetting strengths at the two surfaces and find that the perpendicular morphology or the mixed perpendicular morphology is the equilibrium morphology in a significant portion of the plane. This is in contrast to the simple, strong segregation limit, flat interface theory, which essentially predicts that only parallel morphologies should be observed in (equilibrium) L-thick films.

I. Introduction

The microphase separation of bulk diblock copolymer melts yields periodic structures.[1,2] In this paper, we focus on symmetric and nearly symmetric diblock copolymer melts, which form lamellae with a strongly-selected spatial period L upon bulk microphase separation. For thin films of symmetric diblock copolymers, the interactions at the film surfaces strongly influence the observed morphology due to the high surface area to volume ratio. In this introduction, we first discuss the morphologies observed experimentally in diblock copolymer thin films. We then demonstrate that existing theoretical studies do not adequately explain the experimental results. Finally, we briefly review some theoretical methods for studying diblock copolymers.

In thin films of diblock copolymers, each of the film surfaces usually preferentially favors one of the copolymer species.[3] To maximize the amount of favorable contact, the lamellae should orient parallel to the film (for example, Figure 1a−d), as opposed to perpendicular to the film (Figure 1e). Experimentally, the parallel morphology is usually observed in free-surface thin films, where the film thickness is free to vary.[4−7] Allowing the film thickness to change ensures that the lamellae are free to adopt their equilibrium periodicity and that the preferred species can segregate to each of the two film surfaces. If a film is initially prepared with a thickness incommensurate with any parallel morphology, the film will generally separate upon annealing into regions of different thicknesses, each of which is commensurate with a parallel morphology with the preferred species at each film surface.[6,7] For example, if the equilibrium parallel morphologies require a half-integer film thickness (film thickness of $(i + \frac{1}{2})L$, where L is the equilibrium bulk lamellar period and i is a nonnegative integer), but the film is initially prepared with a thickness of $2L$, the film will, upon annealing, separate into regions of thickness $\frac{3}{2}L$ and $\frac{5}{2}L$.

There are, however, experiments in which a nonparallel morphology is observed in free-surface thin films. We discuss below experiments by Carvalho and Thomas,[8] Henkee et al.,[9] and Morkved and Jaeger.[10,11] Carvalho and Thomas[8] study thin films of (approximately) symmetric polystyrene−PMMA diblock copolymers (molecular weight 108 000 and $\chi N \approx 29$, where χ is the Flory−Huggins parameter describing the degree of polystyrene−PMMA immiscibility and N is the effective number of monomers per polymer) made by placing drops of a dilute solution of the diblock copolymer onto carbon supports and then letting the solvent evaporate. PMMA wets the carbon support, while polystyrene wets the free surface. Because the two film surfaces have opposite preferences for the polymer species, the equilibrium thicknesses consistent with the parallel morphologies are half-integers. As in refs 4−7, Carvalho and Thomas observe parallel morphologies with the expected thicknesses. However, at the steps between parallel morphologies of different thicknesses, transmission electron microscope (TEM) images show that there is a nonparallel morphology.

Henkee et al.[9] study (approximately) symmetric polystyrene−polybutadiene diblock copolymer (molecular weights 41 000 and 87 000) thin films made by placing drops of a dilute solution of the diblock copolymer on carbon-coated glass slides. TEM images are taken before and after annealing. Before annealing, many of the samples exhibit a nonparallel morphology. After annealing, most of the samples adopt parallel morphologies. In some samples, Henkee et al. observe a nonparallel morphology at steps between parallel morphologies of different thicknesses, similar to the observations of Carvalho and Thomas.

Morkved and Jaeger[10,11] study thin films of (approximately) symmetric polystyrene−PMMA diblock copolymers (molecular weight 65 500 and $\chi N \approx 18$) made by spin-coating onto silicon nitride substrates. It is known that PMMA wets the silicon nitride surface, while polystyrene wets the free surface. Since the film surfaces have opposite preferences for the polymer

[†] Current address: Newark Memorial High School, 39375 Cedar Blvd., Newark, CA 94560.

species, these films should, upon annealing, form parallel morphologies with half-integer film thicknesses. When the films are annealed at 155 °C, however, the films exhibit a strong tendency to form regions of thickness L. Moreover, within these L-thick regions, TEM images show that the films adopt a nonparallel morphology.

Morkved and Jaeger hypothesize that the observed nonparallel morphology results from the effective confinement of their films to thickness L, although the mechanism by which effective confinement occurs is not clear. When the film is confined to a predetermined thickness, the simple argument predicting parallel orientation of lamellae (see the first paragraph of the present paper) no longer applies. Confinement means that parallel lamellae may not be able to adopt their preferred periodicity, and the equilibrium morphology depends on the relative free energy penalties for stretching/compressing lamellae and for having unfavorable polymer species at the film surfaces. Morkved and Jaeger perform some calculations which suggest that confined L-thick films can indeed adopt a nonparallel morphology for certain values of the preferential energies at the film surfaces, though the calculations are not rigorous.

Experimentally, nonparallel morphologies have been observed in confined films by Koneripalli et al.[12] and Kellogg et al.[13] Koneripalli et al.[12] study thin films of (approximately) symmetric poly(styrene-d_8)−poly(2-vinylpyridine) diblock copolymers (molecular weight 16 300 and $\chi N \approx 24$) confined between silicon or mica on one side and a glassy homopolymer on the other side. Poly-(2-vinylpyridine) segregates to the silicon or mica surface, while poly(styrene-d_8) segregates to the homopolymer interface. Thus, the equilibrium film thicknesses consistent with the parallel morphologies are half-integers. For films confined to a thickness close to $^3/_2L$, the lamellae orient in the parallel direction. For films confined to a thickness of approximately L, however, TEM images show that the films adopt a nonparallel morphology.

Kellogg et al.[13] investigate the effect of surface energy on confined (approximately) symmetric polystyrene−PMMA diblock copolymers (molecular weight 80 000 and $\chi N \approx 22$). For diblock copolymers confined between SiO_x on one side and SiO_x coated with PMMA on the other side, both confining walls strongly attract PMMA. For diblock copolymers confined by random poly(styrene-r-methyl methacrylate) copolymer layers on both sides, the surface preferential interaction is expected to be weak. In both cases, the equilibrium film thicknesses commensurate with the parallel morphologies are iL, where L is the equilibrium bulk lamellar period and i is a positive integer. For diblock copolymers confined by strongly preferential walls, the lamellae orient in the parallel direction for a range of different film thicknesses. For diblock copolymers confined by random copolymer layers, a nonparallel morphology is observed when the film thickness is about $2.5L$.

We also note that perpendicular lamellae have been observed at the surfaces of bulk diblock copolymers.[14−16] We do not further discuss these experiments since this paper focuses on confined thin films.

Confined symmetric diblock copolymer thin films have also been studied theoretically by Turner,[17] Walton et al.,[18] Kikuchi and Binder,[19] Pickett and Balazs,[20] Sommer et al.,[21] Matsen,[22] and Brown and Chakrabarti.[23]

In addition, Pickett et al.[24] have studied how preferential wetting, nematic interactions, and chain ends influence the orientation of lamellae near a hard wall. Turner[17] considers symmetric diblock copolymers confined between two identical, flat plates. Each of the plates preferentially attracts one of the polymer species. Turner calculates the strong segregation limit free energies for different parallel morphologies as a function of film thickness. Walton et al.[18] extend Turner's strong segregation limit calculations to also include the perpendicular morphology and find that the perpendicular morphology is the equilibrium morphology (lowest in free energy) for certain film thicknesses. Kikuchi and Binder[19] perform Monte Carlo simulations on diblock copolymers confined between two identical, preferential walls. For film thicknesses that are compatible with the bulk lamellar period and the surface interactions, lamellae orient in the parallel direction. For incommensurate film thicknesses, however, Kikuchi and Binder find a perpendicular morphology and a mixed perpendicular morphology containing both parallel and perpendicular lamellae. Pickett and Balazs[20] perform two-dimensional Scheutjens−Fleer calculations (numerical self-consistent field calculations on a spatial lattice) on diblock copolymers ($N = 150$, $\chi N = 15$) confined between two identical walls. They perform two sets of calculations—one for neutral walls and one for preferential walls. For preferential walls, the equilibrium morphology can be a perpendicular or parallel morphology, depending on the film thickness. For neutral walls, the perpendicular morphology is always the equilibrium morphology, regardless of the film thickness. This result for neutral walls is also found by Sommer et al.;[21] in their Monte Carlo simulations of diblock copolymers confined between neutral walls, the perpendicular morphology is the equilibrium morphology.

Matsen[22] uses a numerical continuous space self-consistent field theory to study diblock copolymers confined between two identical walls. The film thicknesses are chosen to be incompatible with the preferred lamellar period and surface interactions; that is, the films are frustrated. (See below for a more complete discussion of frustration.) The free energies of a variety of morphologies are calculated as a function of the strength of the preferential surface potential. For frustrated films of perfectly symmetric diblock copolymers ($\chi N = 20$), the perpendicular morphology and the parallel morphologies are the equilibrium morphologies. The perpendicular morphology is stable for low surface potentials and thin films, while the parallel morphologies are stable for high surface potentials and thick films. For frustrated films of slightly asymmetric diblock copolymers (45:55 ratio of block lengths, instead of 50:50), the perpendicular morphology is stable for low surface potentials, while a mixed perpendicular morphology containing both perpendicular and parallel lamellae is found to be stable for high surface potentials. The mixed perpendicular morphology has parallel lamellae near one wall but perpendicular lamellae near the other wall. The perpendicular lamellae are "capped", where the lamellar orientation changes between perpendicular and parallel, and the tendency of the A−B interface to curve in asymmetric diblock copolymers probably facilitates capping.

Brown and Chakrabarti[23] use a coarse-grained phenomenological model to study confined diblock copolymer films for selected film thicknesses, surface poten-

tials, and temperatures. For films confined by identical walls, the equilibrium morphology is a perpendicular or parallel morphology. For films whose confining walls have equal but opposite preferences for the polymer species, several different morphologies are found. In addition to the perpendicular and parallel morphologies, there are "egg carton" morphologies and twisted perpendicular morphologies (the lamellae rotate by 90° in the middle of the film). However, it is not clear whether these are true equilibrium morphologies rather than metastable states. Moreover, the phenomenological nature of the model makes it difficult to critically evaluate the results.

Thus, nonparallel morphologies are found theoretically under a variety of conditions. Many of the theoretical treatments[18-23] can account for the nonparallel morphology observed by Kellogg et al.[13] for symmetric, (nearly) neutral confining walls. However, none of the theoretical papers described above comprehensively treat the case of confining walls with opposite preferences for the polymer species, as in the experiments of Morkved and Jaeger[10,11] and Koneripalli et al.[12] The nonparallel morphologies found by Brown and Chakrabarti[23] for antisymmetric confining walls are suggestive of the experimental observations of Morkved and Jaeger and Koneripalli et al., but it is not clear under what range of parameters these nonparallel morphologies might be observed. Understanding why nonparallel morphologies form and under what conditions could lead to a variety of practical applications. The patterns formed by the diblock copolymers could be used as a template for structures on the scale of tens to hundreds of nanometers—an order of magnitude smaller than features formed by state of the art lithography in the semiconductor industry.[25,26] However, only nonparallel morphologies are useful as a template; in the parallel morphologies, the film surfaces are homogeneous and thus uninteresting for such applications.

In this paper, we perform a detailed study of thin film morphology. We focus on films with characteristics similar to those of the experimental films of Morkved and Jaeger and Koneripalli et al. for which a nonparallel morphology is observed. Our films have thickness L, where L is the equilibrium bulk lamellar period, and the film surfaces have opposite preferences for the polymer species. We systematically vary the strength of the preferential surface interactions at both film surfaces.

Our films are frustrated; to see this, consider the following qualitative arguments. We denote the two different species in the diblock copolymer as A and B. We label the two surfaces of the film as "bottom" and "top". For convenience, we assume that A wets the bottom surface and B wets the top surface. Some possible morphologies for films of thickness L are shown in Figure 1. In Figure 1a, A is at the bottom surface, which is favorable, and B is at the top surface, which is favorable. However, $1^{1}/_{2}$ full lamellar repeat units (where a full lamellar repeat unit consists of half an A stripe followed by a full B stripe followed by half an A stripe, or vice versa) are forced to fit into the distance L normally occupied by a full lamellar repeat unit. That is, the lamellae are compressed, resulting in a free energy penalty. Similarly, in Figure 1b, A is at the bottom surface, which is favorable, and B is at the top surface, which is favorable, but half a lamellar repeat unit is forced to fit into the distance L normally occupied
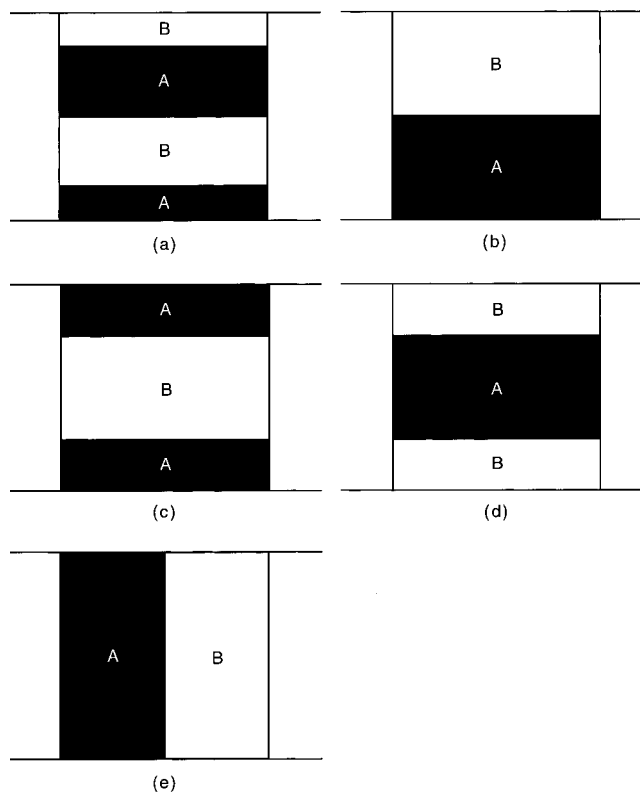

Figure 1. A few possible morphologies for diblock copolymer films of thickness L, where L is the equilibrium bulk lamellar period.

by a full lamellar repeat unit, resulting in a free energy penalty from stretching. In Figure 1c, the lamellae have the equilibrium periodicity, and the interaction at the bottom surface is favorable, but the interaction at the top surface is unfavorable. Similarly, in Figure 1d, the lamellae have the equilibrium periodicity, and the interaction at the top surface is favorable, but the interaction at the bottom surface is unfavorable. Finally, in Figure 1e, the lamellae are free to adopt their equilibrium periodicity since they are perpendicular to the film, but there are unfavorable interactions at both the bottom and the top surfaces. Thus, the system is frustrated; there is no possible way to satisfy all of the conditions for minimizing free energy (A at the bottom surface, B at the top surface, and equilibrium lamellar periodicity). The equilibrium, minimum free energy structure is the morphology with the least frustration, but we cannot predict which of the structures in Figure 1 is the equilibrium structure using only these qualitative arguments.

A simple, commonly used theory for block copolymers is the strong segregation limit theory,[27,28] which assumes that A and B are highly immiscible. Consequently, the lamellae consist of regions of pure A separated from regions of pure B by sharp interfaces. This makes the free energy of all of the morphologies shown in Figure 1 very simple to calculate. (Note that there is a further implicit assumption here—that the A–B interfaces are all flat.) Let $\gamma_{A/bottom}$ be the surface energy per unit area for A at the bottom surface, and similarly for $\gamma_{A/top}$, $\gamma_{B/bottom}$, and $\gamma_{B/top}$. Since we are interested in differences in A and B surface energies, we define $\Delta\gamma_{bottom} = \gamma_{B/bottom} - \gamma_{A/bottom}$ and $\Delta\gamma_{top} = \gamma_{B/top} - \gamma_{A/top}$. Note that the preferential attraction of A to the bottom surface implies that $\Delta\gamma_{bottom} > 0$, while the
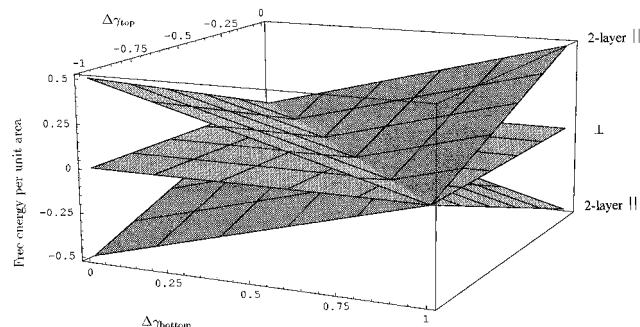
Figure 2. Strong segregation limit free energy per unit area as a function of the preferential surface energies per unit area $\Delta\gamma_{bottom}$ and $\Delta\gamma_{top}$ for the two-layer parallel morphologies, as in Figure 1c (bottom surface at $\Delta\gamma_{bottom} = 0$ and $\Delta\gamma_{top} = -1$; top surface at $\Delta\gamma_{bottom} = 1$ and $\Delta\gamma_{top} = 0$) and Figure 1d (top surface at $\Delta\gamma_{bottom} = 0$ and $\Delta\gamma_{top} = -1$; bottom surface at $\Delta\gamma_{bottom} = 1$ and $\Delta\gamma_{top} = 0$), and the perpendicular morphology, as in Figure 1e (middle surface at $\Delta\gamma_{bottom} = 0$ and $\Delta\gamma_{top} = -1$; middle surface at $\Delta\gamma_{bottom} = 1$ and $\Delta\gamma_{top} = 0$).

preferential attraction of B to the top surface implies that $\Delta\gamma_{top} < 0$. Figure 2 shows the free energy per unit area as a function of $\Delta\gamma_{bottom}$ and $\Delta\gamma_{top}$ for the two-layer parallel morphologies (Figure 1c,d) and the perpendicular morphology (Figure 1e). Since only differences in free energy per area are significant, there is an arbitrary free energy offset for each $\Delta\gamma_{bottom}$ and $\Delta\gamma_{top}$. We choose to set the free energy per area of the perpendicular morphology to be zero for all $\Delta\gamma_{bottom}$ and $\Delta\gamma_{top}$. Figure 2 shows that the perpendicular morphology is lowest in free energy only when $\Delta\gamma_{bottom} = -\Delta\gamma_{top}$, and even then the perpendicular morphology is degenerate with the other two morphologies. However, it is practically impossible to actually find a system with $\Delta\gamma_{bottom}$ exactly equal and opposite to $\Delta\gamma_{top}$ since the line $\Delta\gamma_{bottom} = -\Delta\gamma_{top}$ occupies zero area in the two-dimensional space of $\Delta\gamma_{bottom}$ and $\Delta\gamma_{top}$. Thus, this simple calculation predicts that the perpendicular morphology (Figure 1e) should not be observed (for equilibrium systems). This calculation, however, makes some assumptions that may not hold in experimental systems. All of the thin film morphologies considered in Figure 1 are similar to the bulk morphology—alternating A-rich and B-rich lamellae. However, there is no reason to believe that the thin film morphology must resemble the bulk morphology. In fact, experimental and theoretical studies suggest that, in some cases, the thin film morphology can differ significantly from the bulk morphology. The simple, strong segregation limit, flat interface calculation does not consider such alternative morphologies. Another assumption that often does not hold in real systems is the strong segregation limit assumption of very high A−B immiscibility. The diblock copolymers in the experiments discussed above have $\chi N \approx 20-30$ and are thus far from the strong segregation limit regime (very high χN).

A more sophisticated approach for studying diblock copolymers involves numerically solving the mean field equations.[20,22,29−42] Some of the theoretical approaches discussed above use such an approach.[20,22] In this paper, we use a numerical mean field method originally developed by Scheutjens and Fleer.[38−40] We expect our Scheutjens−Fleer calculations to be more realistic than the simple, strong segregation limit, flat interface calculation since the Scheutjens−Fleer method can treat systems with realistic χN and does not assume that the A−B interface must be flat.

The next section briefly reviews the Scheutjens−Fleer method. We present our results in section III. The significance of our results is discussed in section IV. Finally, section V contains the conclusion.

II. Scheutjens−Fleer Calculations

Scheutjens−Fleer calculations involve numerically solving a set of self-consistent mean field equations on a lattice. These calculations are similar in character to a number of numerical self-consistent field methods.[22,29−37] Scheutjens−Fleer calculations are described in detail in refs 38−40. Our calculations are identical to the two-dimensional generalization described in refs 20, 41, and 42.

The mean field approximation reduces the many-chain problem to a single-chain problem. Instead of treating polymer−polymer interactions directly, we assume that each polymer chain experiences a mean field (potential). The distribution of chain monomers depends on the potential, which in turn depends on the monomer distribution. The monomer distribution and the potential are determined self-consistently. This approximation is similar to the Hartree−Fock self-consistent field approximation, which reduces a many-electron quantum mechanics problem to a single-electron problem.[43] The mean field approximation for treating polymers leads to some anomalous results—for example, the temperature dependence of the Flory−Huggins parameter χ.[44] Nevertheless, the mean field approximation is expected to work well for melts.[45] For bulk diblock copolymer melts, a phase diagram in the $f - \chi N$ plane (where f is the volume fraction of one of the polymer species, χ is the Flory−Huggins parameter, and N is the number of monomers per polymer) has been calculated using the mean field approximation and is in reasonable agreement with experiments.[29,30,33]

Our calculations are performed on a spatial lattice. This discretization approximation is valid only if the quantities calculated vary relatively slowly with respect to the lattice. For diblock copolymers with moderately immiscible A and B blocks (moderate χN), the interface between A-rich and B-rich regions is broad, and the volume fractions of A and B vary relatively slowly in space. However, for diblock copolymers with highly immiscible A and B blocks (large χN), the interface between A-rich and B-rich regions is sharp, and the volume fractions of A and B change rapidly at the interface. Thus, we expect our calculations of the A and B volume fractions to be most accurate for moderate χN.

A polymer molecule is approximated as a flexible chain of monomers. This model works well on a coarse-grained scale. While individual chemical bonds of a polymer molecule are not very flexible since chemical bonds are generally restricted to a small number of conformations, a chain of several bonds appears more flexible. We define an effective monomer to represent a sufficiently long portion of the polymer such that the polymer is approximated well as a chain of highly flexible effective monomers.[46] We number the monomers as $s = 1, 2, ..., N$. Let f be the fraction of the polymer that is species A; monomers numbered $s = 1, 2, ..., fN$ are A, and monomers numbered $s = fN + 1, fN + 2, ..., N$ are B. The degree of immiscibility between A and B monomers is described by the Flory−Huggins parameter χ_{AB}. The interactions of A and B monomers at the film surfaces are similarly described by $\chi_{A/bottom}$, $\chi_{A/top}$, $\chi_{B/bottom}$, and $\chi_{B/top}$. The polymer film is spatially discretized into a cubic lattice. In the direction perpendicular to the film, the lattice sites are labeled $z = 1, 2, ..., m_z$. Parallel to the film, the lattice sites are labeled $x = 1, 2, ..., m_x$. All quantities in the third (y) direction are assumed to be translationally invariant. In the z direction, there are impenetrable walls next to $z = 1$ and $z = m_z$, while periodic boundary conditions are used in the x direction. Let $\phi_A(x, z)$ and $\phi_B(x, z)$ be the volume fractions of A and B at each lattice site. The Flory−Huggins mean field energy (including surface energy) is

$$E/k_B T = \sum_x \sum_z [{}^1\!/_2 \chi_{AB} \phi_A(x, z)(\langle \phi_B(x, z) \rangle - (1 - f)) +$$

$${}^1\!/_2 \chi_{AB} \phi_B(x, z)(\langle \phi_A(x, z) \rangle - f)] + \sum_x [{}^1\!/_6 \chi_{A/bottom} \phi_A(x, 1) +$$

$${}^1\!/_6 \chi_{A/top} \phi_A(x, m_z) + {}^1\!/_6 \chi_{B/bottom} \phi_B(x, 1) + {}^1\!/_6 \chi_{B/top} \phi_B(x, m_z)] \quad (1)$$

where k_B is Boltzmann's constant, T is the temperature, and the nearest-neighbor average $\langle \cdots \rangle$ is defined for any function $h(x, z)$ as

$$\langle h(x, z) \rangle = {}^1\!/_6 h(x, z - 1) + {}^1\!/_6 h(x, z + 1) + {}^1\!/_6 h(x - 1, z) + {}^1\!/_6 h(x + 1, z) + {}^1\!/_3 h(x, z)$$

On a three-dimensional cubic lattice, any lattice site (x, z) has six nearest neighbors. Since we explicitly treat two dimensions and assume translational invariance in the third dimension, two of the nearest neighbors of (x, z) are (x, z) itself. Note that the nearest-neighbor average is *not* the statistical mechanical ensemble average. The system is assumed to be incompressible, which means the A and B volume fractions must satisfy the constraint

$$\phi_A(x, z) + \phi_B(x, z) = 1 \quad (2)$$

The potential $u_A(x, z)$ for A monomers (the energy required to move A monomers from the homogeneous amorphous bulk to the lattice site (x, z) in our system) is given by

$$\frac{u_A(x, z)}{k_B T} = \frac{u'(x, z)}{k_B T} + \chi_{AB}[\langle \phi_B(x, z) \rangle - (1 - f)] +$$

$${}^1\!/_6 \chi_{A/bottom} \delta_{z,1} + {}^1\!/_6 \chi_{A/top} \delta_{z,m_z} \quad (3)$$

where δ_{z1} and δ_{z,m_z} are Kronecker delta functions and $u'(x, z)$ is the "hard-core" potential required for enforcing incompressibility. The potential experienced by B monomers is similarly expressed as

$$\frac{u_B(x, z)}{k_B T} = \frac{u'(x, z)}{k_B T} + \chi_{AB}[\langle \phi_A(x, z) \rangle - f] + {}^1\!/_6 \chi_{B/bottom} \delta_{z,1} +$$

$${}^1\!/_6 \chi_{B/top} \delta_{z,m_z} \quad (4)$$

The Boltzmann weighting factors for A and B monomers are related to the potentials $u_A(x, z)$ and $u_B(x, z)$ by

$$G_A(x, z) = \exp\left[-\frac{u_A(x, z)}{k_B T}\right] \quad (5)$$

$$G_B(x, z) = \exp\left[-\frac{u_B(x, z)}{k_B T}\right] \quad (6)$$

Detached A or B monomers (not part of any polymer) would have a spatial probability distribution given by $G_A(x, z)$ or $G_B(x, z)$, respectively. The connectivity of the polymers is accounted for in the polymer fragment weighting factors $G(x, z, s|1)$ and $G(x, z, s|N)$, where $G(x, z, s|1)$ is defined as the statistical weight of all conformations of the polymer fragment consisting of the first s monomers of the diblock copolymer in which monomer s is located at lattice site (x, z) and monomer 1 can be located anywhere, and $G(x, z, s|N)$ is defined as the statistical weight of all conformations of the polymer fragment consisting of the last $N - s + 1$ monomers of the diblock copolymer in which monomer s is located at lattice site (x, z) and monomer N can be located anywhere. To calculate $G(x, z, s|1)$, we notice that for monomer s ($s > 1$) to be located at the lattice site (x, z), monomer $s - 1$ must be located at a neighbor lattice site $((x - 1, z), (x + 1, z), (x, z - 1), (x, z + 1),$ or $(x, z))$. Thus, $G(x, z, s|1)$ is proportional to the nearest-neighbor average $\langle G(x, z, s - 1|1) \rangle$. Placing monomer s at the lattice

site (x, z) contributes a factor $G_A(x, z)$ or $G_B(x, z)$, depending on whether monomer s is an A monomer or a B monomer. Therefore, $G(x, z, s|1)$ can be computed recursively

for $s = 1$: $\quad G(x, z, s|1) = G_A(x, z)$

for $s = 2, \ldots, N$:

$$G(x, z, s|1) = \begin{cases} G_A(x, z), & \text{if } s \le fN \\ G_B(x, z), & \text{if } s > fN \end{cases} \times \langle G(x, z, s - 1|1) \rangle \quad (7)$$

Similarly, $G(x, z, s|N)$ is computed by

for $s = N$: $\quad G(x, z, s|N) = G_B(x, z)$

for $s = N - 1, \ldots, 1$:

$$G(x, z, s|N) = \begin{cases} G_A(x, z), & \text{if } s \le fN \\ G_B(x, z), & \text{if } s > fN \end{cases} \times \langle G(x, z, s + 1|N) \rangle \quad (8)$$

The volume fraction $\phi(x, z, s)$ at lattice site (x, z) of monomer s of the entire diblock copolymer of length N can be calculated from the polymer fragment weighting factors $G(x, z, s|1)$, which corresponds to the fragment from monomer 1 to monomer s, and $G(x, z, s|N)$, which corresponds to the fragment from monomer s to monomer N

$$\phi(x, z, s) = \begin{cases} \dfrac{1}{N} \dfrac{G(x, z, s|1)\, G(x, z, s|N)}{G_A(x, z)}, & \text{if } s \le fN \\[3mm] \dfrac{1}{N} \dfrac{G(x, z, s|1)\, G(x, z, s|N)}{G_B(x, z)}, & \text{if } s > fN \end{cases} \quad (9)$$

The denominator $G_A(x, z)$ or $G_B(x, z)$ compensates for double-counting since monomer s is accounted for in both $G(x, z, s|1)$ and $G(x, z, s|N)$, and $1/N$ is a normalization factor. The total A and B volume fractions are given by

$$\phi_A(x, z) = \sum_{s=1}^{fN} \phi(x, z, s) = \frac{1}{N} \sum_{s=1}^{fN} \frac{G(x, z, s|1)\, G(x, z, s|N)}{G_A(x, z)} \quad (10)$$

$$\phi_B(x, z) = \sum_{s=fN+1}^{N} \phi(x, z, s) = \frac{1}{N} \sum_{s=fN+1}^{N} \frac{G(x, z, s|1)\, G(x, z, s|N)}{G_B(x, z)} \quad (11)$$

In any consistent solution, $\phi_A(x, z)$ and $\phi_B(x, z)$ computed in eqs 10 and 11 must agree with the $\phi_A(x, z)$ and $\phi_B(x, z)$ in eqs 3 and 4. Furthermore, $\phi_A(x, z)$ and $\phi_B(x, z)$ must satisfy the incompressibility constraint 2. Thus, eqs 2−11 form a self-consistent set of $3m_x m_z$ equations[47] in the $3m_x m_z$ unknowns $\phi_A(x, z)$, $\phi_B(x, z)$, and $u'(x, z)$; $x = 1, \ldots, m_x$, $z = 1, \ldots, m_z$. These equations can be solved numerically by routines for nonlinear algebraic equations.[48,49]

The total energy is calculated from eq 1. The entropy is given by[50]

$$S/k_B = -\sum_x \sum_z [\phi_A(x, z) \ln G_A(x, z) + \phi_B(x, z) \ln G_B(x, z)] \quad (12)$$

Finally, the free energy is given by

$$\frac{F}{k_B T} = \frac{E - TS}{k_B T} = \sum_x \sum_z [\phi_A(x, z) \ln G_A(x, z) +$$

$$\phi_B(x, z) \ln G_B(x, z) + {}^1\!/_2 \chi_{AB} \phi_A(x, z)(\langle \phi_B(x, z) \rangle - (1 - f)) +$$

$${}^1\!/_2 \chi_{AB} \phi_B(x, z)(\langle \phi_A(x, z) \rangle - f)] + \sum_x [{}^1\!/_6 \chi_{A/bottom} \phi_A(x, 1) +$$

$${}^1\!/_6 \chi_{A/top} \phi_A(x, m_z) + {}^1\!/_6 \chi_{B/bottom} \phi_B(x, 1) + {}^1\!/_6 \chi_{B/top} \phi_B(x, m_z)] \quad (13)$$

The solutions we obtain depend on the initial guesses for $\phi_A(x, z)$, $\phi_B(x, z)$, and $u'(x, z)$ as well as the iteration procedure for approaching the final solution. We are primarily interested

in the lowest free energy solutions. We perform the calculations using a variety of initial conditions, but it is possible that we missed some low free energy solutions.

We do a few calculations to verify the accuracy of our method. The analytical, weak segregation limit theory[51] predicts that, for symmetric ($f = 0.5$) diblock copolymers with large N, the microphase separation transition from the disordered phase to the lamellar phase should occur at $\chi N \approx 10.5$, and our calculations reproduce this transition value. In addition, our calculations reproduce results reported in ref 20. Our coding of the Scheutjens–Fleer equations was independent of ref 20, and presumably, our iteration procedure was different as well. Nevertheless, our computed free energies match those of Figure 2 in ref 20 exactly. For example, we calculate a free energy of 0.3776 for a film thickness of 13, and this agrees with the data in Figure 2 of ref 20 to at least $3^1/_2$ decimal places. We obtain similar agreement with 16 other data points reported in Figure 2 of ref 20.[52]

Our results are reported with $\Delta\chi_{bottom} = \chi_{B/bottom} - \chi_{A/bottom}$ and $\Delta\chi_{top} = \chi_{B/top} - \chi_{A/top}$ expressed in units of $k_B T$. Converting $\Delta\chi_{bottom}$ and $\Delta\chi_{top}$ to differences in surface tension, which can be measured experimentally, requires knowledge of the volume associated with each lattice site. For a typical polymer, the volume displaced by a statistical segment is on the order of 1000 Å^3,[53,54] which leads to a lattice area of about 100 Å^2. At a temperature T of 150 °C, a $\Delta\chi_{bottom}$ or $\Delta\chi_{top}$ of 1 $k_B T$ corresponds to a difference in surface tension of about 1 dyn/cm.

We study films of thickness approximately L, where L is the bulk equilibrium period. To determine L, we perform calculations on a range of lattice sizes. The lattice which produces the lowest free energy per chain has the appropriate size and is commensurate with L.

We have performed calculations on L-thick films with varying lattice sizes in the direction parallel to the film surfaces. (Recall that there are periodic boundary conditions in this direction.) For parallel morphologies, the free energy per unit area of film is independent of lattice size parallel to the film surfaces, as expected. For nonparallel morphologies, the free energy per unit area is lowest when the lattice size parallel to the film surfaces is commensurate with L. Thus, in the discussion below, the only results presented are for calculations in which the lattice size parallel to the film surfaces is L.

III. Results

Figure 3 shows the results of Scheutjens–Fleer calculations for L-thick films with $\chi N = 20$, $N = 80$, and $f = 0.5$ (equal fractions of A and B in the diblock copolymer). The calculations use a 15×15 lattice for this N and χN, since the bulk equilibrium period L is 15 lattice sites. Parts a and b of Figure 3 show the free energy per unit area as a function of $\Delta\chi_{bottom} = \chi_{B/bottom} - \chi_{A/bottom}$ and $\Delta\chi_{top} = \chi_{B/top} - \chi_{A/top}$. Since we are interested in systems in which A wets the bottom surface and B wets the top surface, $\Delta\chi_{bottom} > 0$ and $\Delta\chi_{top} < 0$. Figure 3a shows the free energy per area for the perpendicular morphology (Figure 1e) and the two-layer parallel morphologies (Figure 1c,d). For the two-layer parallel morphologies, to avoid clutter, only the lower of the free energies per area is shown. Figure 3b shows the free energy per area for the perpendicular morphology (Figure 1e) and the three-layer parallel morphology. The free energy graph for the one-layer parallel morphology (Figure 1b) is similar to that for the three-layer parallel morphology but is much higher in free energy and is thus not shown. As discussed previously for the strong segregation limit free energy plotted in Figure 2, there is an arbitrary free energy offset for each $\Delta\chi_{bottom}$ and $\Delta\chi_{top}$. In Figure 3, the offsets are chosen so that the strong segregation limit, flat interface perpen-

dicular morphology (*not* shown in Figure 3) would have a constant (but nonzero) free energy per area. We note that the graphs are symmetric about $\Delta\chi_{top} = -\Delta\chi_{bottom}$ because the diblock copolymers are symmetric—equal fractions of A and B. Figure 3c shows the range of values for $\Delta\chi_{bottom}$ and $\Delta\chi_{top}$ for which the different morphologies are lowest in free energy.[55] In the upper right and lower left corners, the two-layer parallel morphologies are the lowest in free energy. In the lower right corner, the three-layer parallel morphology is the equilibrium morphology. In the remaining region, which encompasses the $\Delta\chi_{top} = -\Delta\chi_{bottom}$ line for small $|\Delta\chi_{bottom}|$ and $|\Delta\chi_{top}|$, the perpendicular morphology is the equilibrium structure. Thus, Scheutjens–Fleer calculations predict a much larger region of stability than that predicted by the strong segregation limit, flat interface calculation. We now explore the reasons for these differing predictions.

We first consider the system with neutral bottom and top surfaces ($\Delta\chi_{bottom} = \Delta\chi_{top} = 0$). In the strong segregation limit, flat interface calculation, the perpendicular morphology and the two-layer parallel morphology are degenerate in free energy. In the Scheutjens–Fleer calculations, however, the perpendicular morphology is lower in free energy than the two-layer parallel morphology. This difference appears to arise in part from wall-induced A–B compatibilization.[22,56] Any monomer next to a wall has fewer neighboring monomers than a monomer away from the wall. On our cubic lattice, a monomer away from the wall has six nearest (monomer) neighbors, but a monomer next to the wall only has five nearest (monomer) neighbors, with the sixth nearest-neighbor site being occupied by the wall. Thus, a monomer next to the wall has a lesser impact on the total energy than a monomer away from the wall. (Calculating the total energy involves taking nearest-neighbor averages; we ignore the surface energy terms since the walls are neutral. See eq 1.) In effect, a monomer next to the wall appears to have a lower χ_{AB} than a monomer away from the wall. Since the perpendicular morphology has more unfavorable A–B contacts in the layer next to the wall than the two-layer parallel morphology (see Figure 1), the decrease in the effective χ_{AB} next to the wall lowers the free energy of the perpendicular morphology more than the two-layer parallel morphology. If we do a calculation in which the nearest-neighbor average is replaced by the local value only, thereby eliminating the effective decrease of χ_{AB} near the wall, most of the difference in free energy between the two morphologies disappears. For $\chi N = 20$, $N = 80$, $f = 0.5$, and $\Delta\chi_{bottom} = \Delta\chi_{top} = 0$, the difference in free energy between the two-layer parallel morphologies and the perpendicular morphology is $0.006 k_B T$ per lattice area for the nearest-neighbor average calculation and is $-0.001 k_B T$ per lattice area for the local value calculation. The residual free energy difference may be attributed to other effects, such as the chain end effect[20,24] or changes in chain entropy near walls.

Another characteristic of the Scheutjens–Fleer method is that the calculated film structure, as given by $\phi_A(x, z)$, changes as $\Delta\chi_{bottom}$ and $\Delta\chi_{top}$ change. In contrast, the strong segregation limit, flat interface calculation assumes that the film structure remains the same when $\Delta\chi_{bottom}$ and $\Delta\chi_{top}$ change. Figure 4 compares the free energy per area calculated by the Scheutjens–Fleer method against a reference free energy per area obtained by assuming that the film structure is invariant
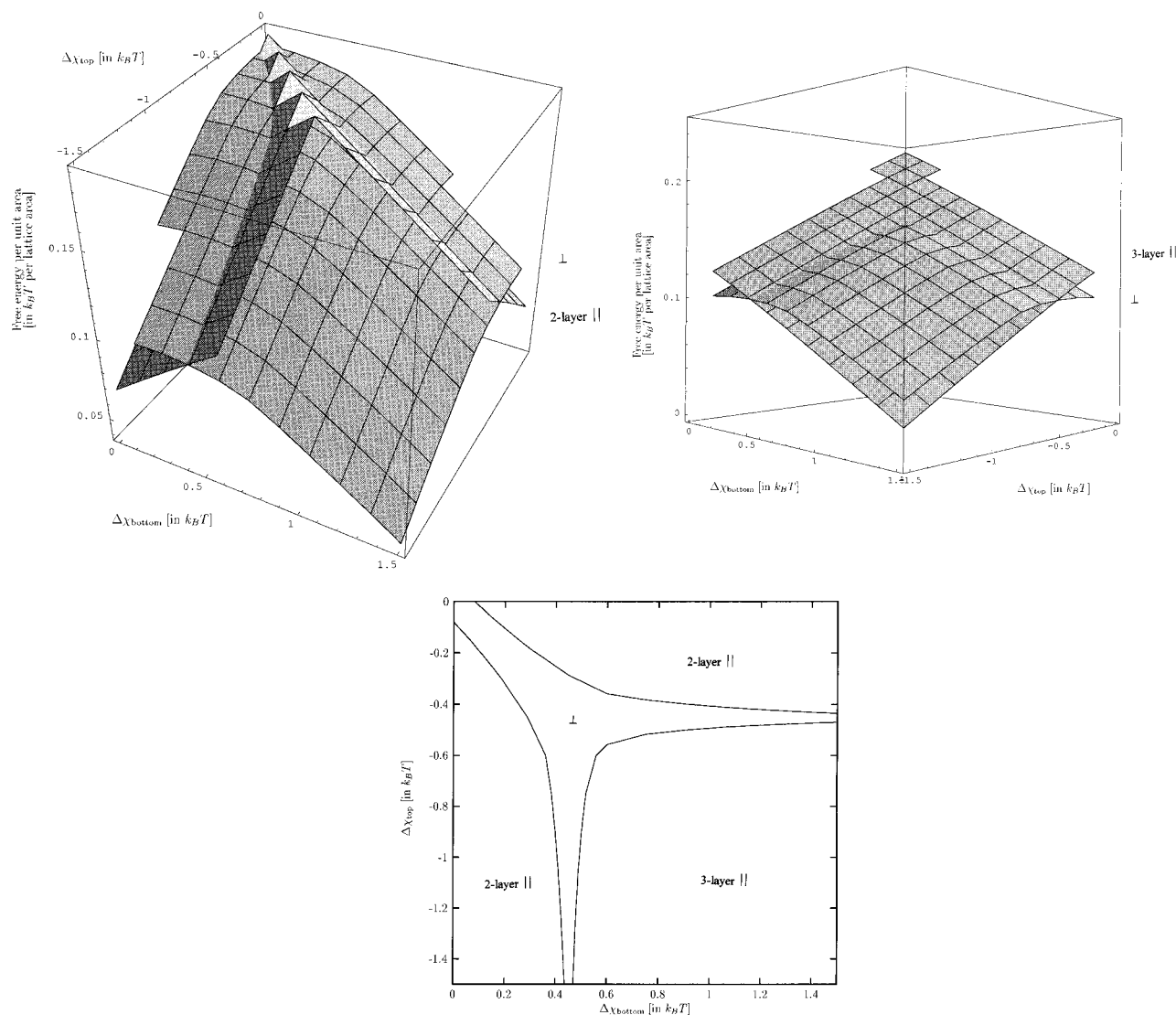
Figure 3. (a, top left) Scheutjens−Fleer free energy per unit area as a function of the preferential surface interactions $\Delta\chi_{bottom}$ and $\Delta\chi_{top}$ for the two-layer parallel morphologies (top surface at $\Delta\chi_{bottom} = \Delta\chi_{top} = 0$; bottom surface at $\Delta\chi_{bottom} = 0.15$ and $\Delta\chi_{top} = -1.5$), as in Figure 1c,d, and the perpendicular morphology (bottom surface at $\Delta\chi_{bottom} = \Delta\chi_{top} = 0$; top surface at $\Delta\chi_{bottom} = 0.15$ and $\Delta\chi_{top} = -1.5$), as in Figure 1e or 5. The calculations are done for $\chi N = 20$, $N = 80$, and $f = 0.5$ on a 15×15 lattice. (b, top right) Scheutjens−Fleer free energy per unit area as a function of the preferential surface interactions $\Delta\chi_{bottom}$ and $\Delta\chi_{top}$ for the three-layer parallel morphology (top surface at $\Delta\chi_{bottom} = \Delta\chi_{top} = 0$; bottom surface at $\Delta\chi_{bottom} = 1.5$ and $\Delta\chi_{top} = -1.5$), as in Figure 1a, and the perpendicular morphology (bottom surface at $\Delta\chi_{bottom} = \Delta\chi_{top} = 0$; top surface at $\Delta\chi_{bottom} = 1.5$ and $\Delta\chi_{top} = -1.5$), as in Figure 1e or 5. The calculations are done for $\chi N = 20$, $N = 80$, and $f = 0.5$ on a 15×15 lattice. (c, bottom) Phase diagram showing the regions of stability for different morphologies for $\chi N = 20$, $N = 80$, $f = 0.5$, and film thicknesses of 15 lattice sites. The two-layer parallel morphologies (as in Figure 1c,d) are stable in the upper right and lower left corners. The three-layer parallel morphology (as in Figure 1a) is stable in the lower right corner. The perpendicular morphology (as in Figure 1e or 5) is stable in the remaining region: $\Delta\chi_{bottom} \approx -\Delta\chi_{top}$ for small $|\Delta\chi_{bottom}|$ and $|\Delta\chi_{top}|$, $\Delta\chi_{top} \approx -0.45$ and large $\Delta\chi_{bottom}$, and $\Delta\chi_{bottom} \approx 0.45$ and large, negative $\Delta\chi_{top}$.

under changes in $\Delta\chi_{bottom}$ and $\Delta\chi_{top}$. More precisely, the reference free energy per area for all $\Delta\chi_{bottom}$ and $\Delta\chi_{top}$ is calculated using the Scheutjens−Fleer film structure for $\Delta\chi_{bottom} = \Delta\chi_{top} = 0$. Figure 4 shows that allowing the film structure to vary as $\Delta\chi_{bottom}$ and $\Delta\chi_{top}$ vary does not have a significant effect for the two-layer and three-layer parallel morphologies but has a large effect for the perpendicular morphology. The reason for the large effect can be seen in Figure 5. For different values of $\Delta\chi_{bottom}$ and $\Delta\chi_{top}$, $\phi_A(x, z)$ can differ dramatically. In Figure 5a, the $\phi_A(x, z)$ profile is very similar to the ϕ_A-(x, z) profile of bulk diblock copolymer, while in Figure 5b, the high value of $\Delta\chi_{bottom}$ leads to a novel structure with increased $\phi_A(x, z)$ near the bottom surface. Similarly, in Figure 5c, the large, negative value of $\Delta\chi_{top}$

leads to increased $\phi_B(x, z)$ (decreased $\phi_A(x, z)$) near the top surface.

In summary, the Scheutjens−Fleer method accounts for wall-induced A−B compatibilization and the variation of the film structure under changes in $\Delta\chi_{bottom}$ and $\Delta\chi_{top}$. Both of these effects lower the free energy of the perpendicular morphology relative to the free energy of the parallel morphologies and lead to a greatly increased region of stability for the perpendicular morphology. Our calculations confirm and extend results observed in similar self-consistent field calculations.[20,22]

We now investigate the effect of changing film thickness, the asymmetry parameter f, N, and χN. We first consider film thickness. Figure 6 shows the regions of stability for the different morphologies for $\chi N = 20$, N
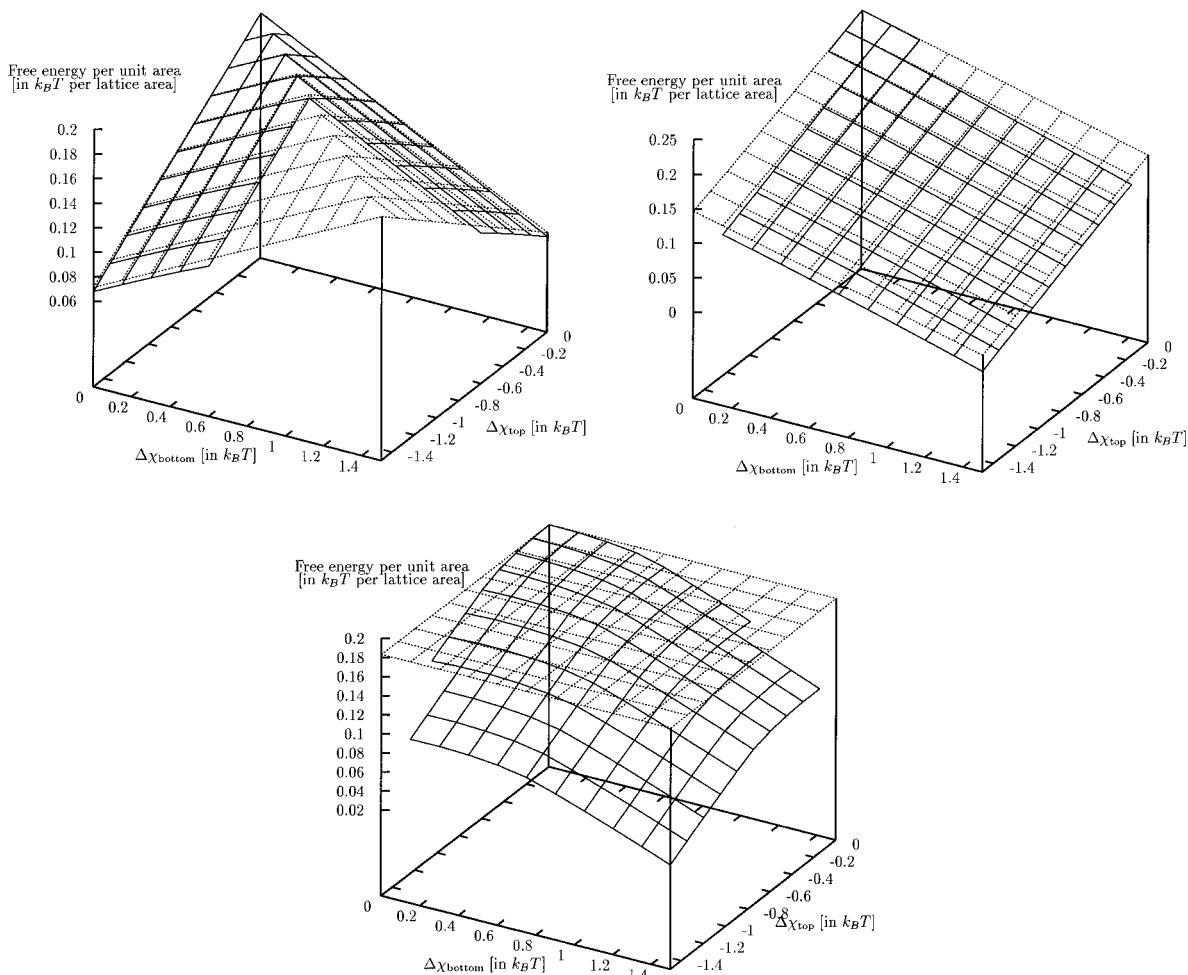
Figure 4. (a, top left) Comparison of the Scheutjens–Fleer free energy per unit area (solid lines) versus a reference free energy per unit area (dotted lines) for the two-layer parallel morphologies, as in Figure 1c,d. The reference free energy is calculated by using the film structure for $\Delta\chi_{bottom} = \Delta\chi_{top} = 0$ (neutral surfaces) to calculate a free energy for all $\Delta\chi_{bottom}$ and $\Delta\chi_{top}$. The calculations are done for $\chi N = 20$, $N = 80$, and $f = 0.5$ on a 15×15 lattice. (b, top right) Comparison of the Scheutjens–Fleer free energy per unit area (solid lines) versus a reference free energy per unit area (dotted lines) for the three-layer parallel morphology, as in Figures 1e. The reference free energy is calculated by using the film structure for $\Delta\chi_{bottom} = \Delta\chi_{top} = 0$ (neutral surfaces) to calculate a free energy for all $\Delta\chi_{bottom}$ and $\Delta\chi_{top}$. The calculations are done for $\chi N = 20$, $N = 80$, and $f = 0.5$ on a 15×15 lattice. (c, bottom) Comparison of the Scheutjens–Fleer free energy per unit area (solid lines) versus a reference free energy per unit area (dashed lines) for the perpendicular morphology, as in Figure 1e. The reference free energy is calculated by using the film structure for $\Delta\chi_{bottom} = \Delta\chi_{top} = 0$ (neutral surfaces) to calculate a free energy for all $\Delta\chi_{bottom}$ and $\Delta\chi_{top}$. The calculations are done for $\chi N = 20$, $N = 80$, and $f = 0.5$ on a 15×15 lattice.

$= 80$, $f = 0.5$, and film thicknesses of 14, 15 (equilibrium), and 16 lattice sites. The boundary between the perpendicular morphology and the three-layer parallel morphology regions of stability is very sensitive to changes in film thickness, while the boundary between the perpendicular morphology and the two-layer parallel morphology regions of stability is relatively insensitive to changes in film thickness. This contrasting behavior can be understood by considering two different effects. While we expect the perpendicular morphology to be fairly insensitive to changes in film thickness, the free energies of the parallel morphologies are affected by changes in film thickness. Changing the film thickness distorts the lamellar period of the three-layer parallel morphology more than the two-layer parallel morphology and results in a larger displacement of the free energy surface of the three-layer parallel morphology than the two-layer parallel morphology. The second effect considers the relative slopes of the free energy surfaces. Figure 3b shows that the free energy surfaces of the perpendicular and the three-layer parallel mor-

phologies have similar slopes where they intersect. The three-layer parallel morphology has predominantly A at the bottom surface and predominantly B at the top surface. For large $\Delta\chi_{bottom}$ and moderate, negative $\Delta\chi_{top}$, the perpendicular morphology has predominantly A at the bottom surface, as illustrated in Figure 5b, and approximately equal amounts of A and B at the top surface. Thus, for large $\Delta\chi_{bottom}$ and moderate, negative $\Delta\chi_{top}$, the free energy surfaces for the three-layer parallel and perpendicular morphologies have nearly identical slopes with respect to $\Delta\chi_{bottom}$ and somewhat similar slopes with respect to $\Delta\chi_{top}$. Similarly, for moderate $\Delta\chi_{bottom}$, and large, negative $\Delta\chi_{top}$ the perpendicular morphology has approximately equal amounts of A and B at the bottom surface and predominantly B at the top surface. Thus, for moderate $\Delta\chi_{bottom}$, and large, negative $\Delta\chi_{top}$, the free energy surfaces for the three-layer parallel and perpendicular morphologies have somewhat similar slopes with respect to $\Delta\chi_{bottom}$ and nearly identical slopes with respect to $\Delta\chi_{top}$. The similarity in slopes of the two free energy surfaces
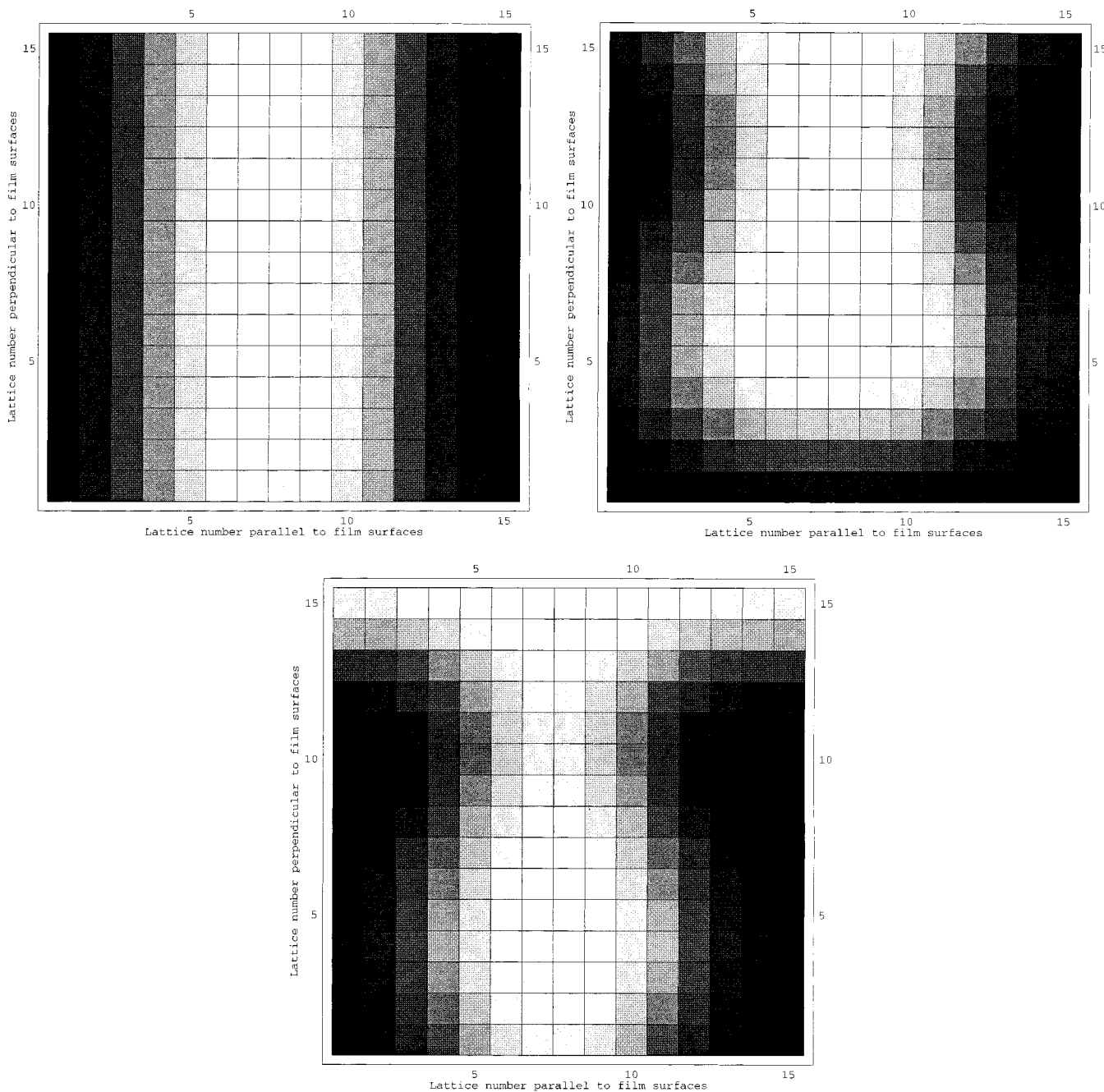
Figure 5. (a, top left) Density plot of the A volume fraction ϕ_A for the perpendicular morphology for $\Delta\chi_{bottom} = \Delta\chi_{top} = 0$ (neutral surfaces). The dark areas represent regions of high ϕ_A, while the light areas represent regions of low ϕ_A. The film surfaces are at the bottom and top of this figure, and there are periodic boundary conditions in the horizontal direction. The view in this plot is similar to that in Figure 1c. The calculations are done for $\chi N = 20$, $N = 80$, and $f = 0.5$ on a 15×15 lattice. (b, top right) Density plot of the A volume fraction ϕ_A for the perpendicular morphology for $\Delta\chi_{bottom} = 0.9$ and $\Delta\chi_{top} = -0.45$. The dark areas represent regions of high ϕ_A, while the light areas represent regions of low ϕ_A. The film surfaces are at the bottom and top of this figure, and there are periodic boundary conditions in the horizontal direction. The view in this plot is similar to that in Figure 1c. The calculations are done for $\chi N = 20$, $N = 80$, and $f = 0.5$ on a 15×15 lattice. (c, bottom) Density plot of the A volume fraction ϕ_A for the perpendicular morphology for $\Delta\chi_{bottom} = 0.45$ and $\Delta\chi_{top} = -0.9$. The dark areas represent regions of high ϕ_A, while the light areas represent regions of low ϕ_A. The film surfaces are at the bottom and top of this figure, and there are periodic boundary conditions in the horizontal direction. The view in this plot is similar to that in Figure 1c. The calculations are done for $\chi N = 20$, $N = 80$, and $f = 0.5$ on a 15×15 lattice.

where they intersect means that small changes in the displacement between the two surfaces arising from small changes in film thickness lead to large changes in the location of the boundary line. On the other hand, in Figure 3a, the free energy surfaces of the perpendicular and the two-layer parallel morphologies have sufficiently different slopes so that the location of the boundary line is relatively insensitive to changes in the displacement between the two surfaces. Together, the

two effects can account for the sensitivity of the boundary between the perpendicular morphology and the three-layer parallel morphology to changes in film thickness and the contrasting insensitivity of the boundary between the perpendicular morphology and the two-layer parallel morphologies to changes in film thickness.

Figure 7 shows the effect of a small amount of asymmetry in the diblock copolymers. The parameters for Figure 7 are the same as for Figure 6, except *f*, the
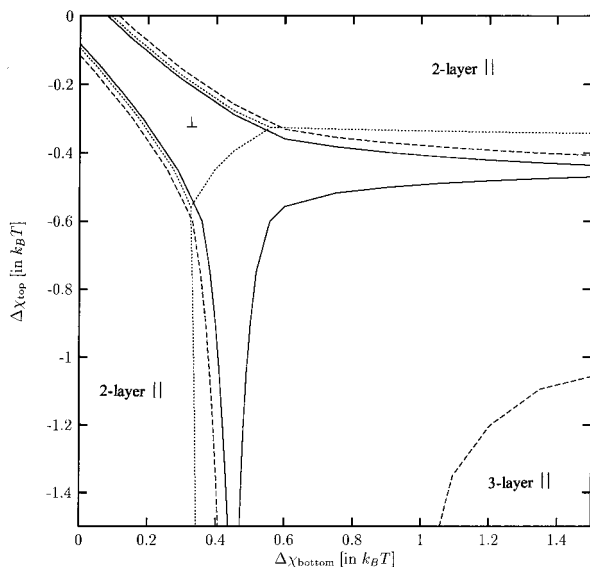
Figure 6. Phase diagram showing the regions of stability for different morphologies for $\chi N = 20$, $N = 80$, $f = 0.5$, and film thicknesses of 14 (dashed lines), 15 (solid lines), and 16 (dotted lines) lattice sites. The two-layer parallel morphologies (as in Figure 1c,d) are stable in the upper right and lower left corners. The three-layer parallel morphology (as in Figure 1a) is stable in the lower right corner. The perpendicular morphology (as in Figures 1e or 5) is stable in the remaining region: $\Delta\chi_{bottom} \approx -\Delta\chi_{top}$ for small $|\Delta\chi_{bottom}|$ and $|\Delta\chi_{top}|$, $\Delta\chi_{top} \approx -0.45$ and large $\Delta\chi_{bottom}$ (film thickness of 14 or 15), and $\Delta\chi_{bottom} \approx 0.45$ and large, negative $\Delta\chi_{top}$ (film thickness of 14 or 15).

fraction of the diblock copolymer that is species A, has been decreased from 0.5 (perfect symmetry, i.e., equal amounts of A and B) to 0.45 (more B than A). This A–B asymmetry destroys the symmetry about the $\Delta\chi_{top} = -\Delta\chi_{bottom}$ line. Having excess B facilitates the formation of structures such as that in Figure 5c, where there is extra B near the top surface. This lowers the free energy of the perpendicular morphology in systems with large, negative $\Delta\chi_{top}$ (the top surface strongly prefers B over A) and thus enlarges the region of stability for the perpendicular morphology for large, negative $\Delta\chi_{top}$. Conversely, having a deficit of A makes it more difficult to form structures with extra A at the bottom surface, as in Figure 5b. This raises the free energy of the perpendicular morphology in systems with large $\Delta\chi_{bottom}$ (the bottom surface strongly prefers A over B) and thus shrinks the region of stability for the perpendicular morphology for large $\Delta\chi_{bottom}$.

An alternative way of understanding the role of asymmetry is to note that asymmetry in diblock copolymers tends to induce curvature in the A–B interface. A bulk sample of perfectly symmetric diblock copolymers forms lamellae free of curvature strain. Slightly asymmetric diblock copolymers have a tendency to curve the A–B interface, but packing considerations keep the bulk sample in the lamellar morphology. For sufficiently large asymmetry, the tendency to curve leads to the formation of an alternative morphology—a cylindrical morphology or a more complex bicontinuous morphology. In the mean field approximation, for $\chi N \approx 20$, the asymmetry for which the lamellar phase becomes unstable is $f \approx 0.38$;[29,30,33] thus, bulk diblock copolymers with $\chi N = 20$ and $f = 0.45$ adopt the lamellar morphology. In the thin film, an asymmetry of $f = 0.45$ by itself cannot induce enough curvature to cause a large deviation from the lamellar morphology; for $\Delta\chi_{bottom} = \Delta\chi_{top}$

$= 0$, the thin film structure resembles the bulk lamellar structure. However, this asymmetry, which causes a tendency for the A–B interface to curve toward the A block, enhances the ability of preferential interactions at the top surface to induce the formation of structures with excess B near the top surface. (See Figure 5c.) Similarly, the asymmetry inhibits the ability of preferential interactions at the bottom surface to induce the formation of structures with excess A at the bottom surface.

Figure 7 also shows that thin films of slightly asymmetric diblock copolymers exhibit a novel equilibrium morphology not seen in thin films of perfectly symmetric diblock copolymers. This mixed perpendicular morphology, whose structure is shown in Figure 8, is stable for large $\Delta\chi_{bottom}$ and moderate, negative $\Delta\chi_{top}$. In the bottom half of the film, the mixed perpendicular morphology is similar to the two-layer parallel morphology. The large $\Delta\chi_{bottom}$ makes it favorable to have A at the bottom surface. Thus, there is an A layer of thickness approximately $^1/_4 L$ at the bottom surface, followed by a B layer of thickness approximately $^1/_4 L$. In the top half of the film, the mixed perpendicular morphology is similar to the perpendicular morphology. Having more B than A ($f < 0.5$) results in a tendency for the A–B interface to curve toward the A block and facilitates the transition from parallel lamellae in the bottom half of the film to perpendicular lamellae in the top half of the film.

Figure 9 shows the regions of stability for different morphologies for $\chi N = 20$ and $N = 40$; for $\chi N = 20$ and $N = 40$, the bulk equilibrium period is 11 lattice sites. Figure 10 shows the regions of stability for different morphologies for $\chi N = 30$ and $N = 80$; for $\chi N = 30$ and $N = 80$, the bulk equilibrium period is 17 lattice sites. Figures 9 and 10 demonstrate that the qualitative features of Figures 6 and 7 do not change significantly when N is decreased from 80 to 40 or χN is increased from 20 to 30. Thus, much of the above discussion for $\chi N = 20$ and $N = 80$ is applicable to a range of χN and N.

IV. Discussion

It is often assumed that the structure of diblock copolymer thin films is similar to the structure of bulk diblock copolymer. Our calculations, like several preceding ones, demonstrate that this assumption does not always hold. While the thin film parallel morphologies are generally well-approximated by slicing bulk diblock copolymer along the direction parallel to the lamellae and compressing or stretching as necessary, the perpendicular morphology can differ greatly from the structure obtained by simply slicing bulk diblock copolymer along the direction perpendicular to the lamellae. For large $\Delta\chi_{bottom}$ (the bottom surface strongly attracts A), the perpendicular morphology exhibits a large increase of A near the bottom surface compared to the naive structure obtained by slicing bulk diblock copolymer. (See Figure 5b.) Similarly, for large, negative $\Delta\chi_{top}$ (the top surface strongly attracts B), the perpendicular morphology exhibits an increase of B near the top surface. (See Figure 5c.) The structural adaptation of the perpendicular morphology together with wall-induced A–B compatibilization lowers the free energy of the perpendicular morphology relative to the free energy of the parallel morphologies and increases the region of stability for the perpendicular morphology. In
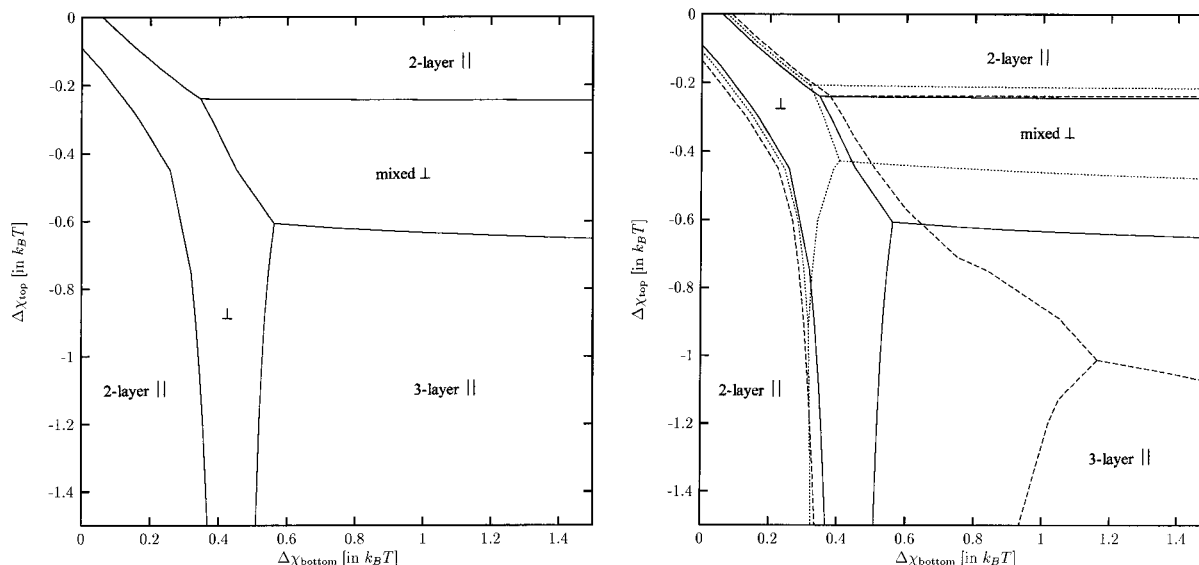
Figure 7. (a, left) Phase diagram showing the regions of stability for different morphologies for $\chi N = 20$, $N = 80$, $f = 0.45$, and film thicknesses of 15 lattice sites. The two-layer parallel morphologies (as in Figure 1c,d) are stable in the upper right and lower left corners. The three-layer parallel morphology (as in Figure 1a) is stable in the lower right corner. The perpendicular morphology (as in Figures 1e or 5) is stable for $\Delta\chi_{\text{bottom}} \approx -\Delta\chi_{\text{top}}$ for small $|\Delta\chi_{\text{bottom}}|$ and $|\Delta\chi_{\text{top}}|$, and $\Delta\chi_{\text{bottom}} \approx 0.4$ and large, negative $\Delta\chi_{\text{top}}$. The mixed perpendicular morphology (as in Figure 8) is stable for $\Delta\chi_{\text{top}} \approx -0.4$ and large $\Delta\chi_{\text{bottom}}$. (b, right) Phase diagram showing the regions of stability for different morphologies for $\chi N = 20$, $N = 80$, $f = 0.45$, and film thicknesses of 14 (dashed lines), 15 (solid lines), and 16 (dotted lines) lattice sites. The two-layer parallel morphologies (as in Figure 1c,d) are stable in the upper right and lower left corners. The three-layer parallel morphology (as in Figure 1a) is stable in the lower right corner. The perpendicular morphology (as in Figures 1e or 5) is stable for $\Delta\chi_{\text{bottom}} \approx -\Delta\chi_{\text{top}}$ for small $|\Delta\chi_{\text{bottom}}|$ and $|\Delta\chi_{\text{top}}|$, and $\Delta\chi_{\text{bottom}} \approx 0.4$ and large, negative $\Delta\chi_{\text{top}}$. The mixed perpendicular morphology (as in Figure 8) is stable for $\Delta\chi_{\text{top}} \approx -0.4$ and large $\Delta\chi_{\text{bottom}}$.
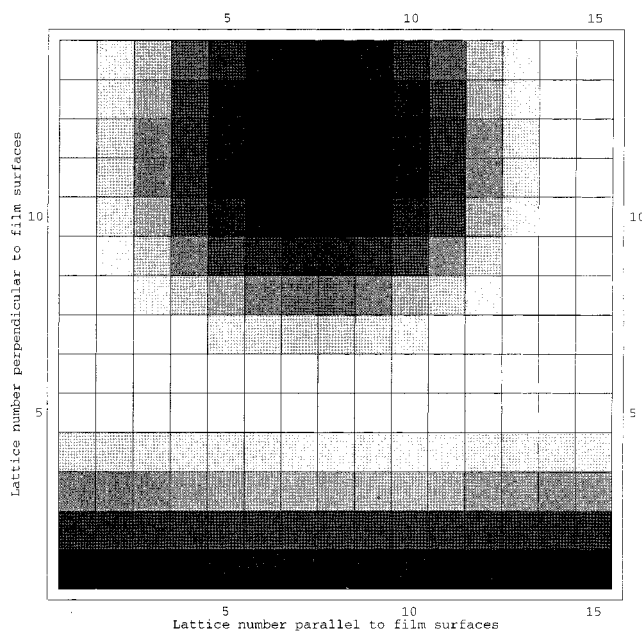

Figure 8. Density plot of the A volume fraction ϕ_A for the mixed perpendicular morphology for $\Delta\chi_{\text{bottom}} = 0.9$ and $\Delta\chi_{\text{top}} = -0.45$. The dark areas represent regions of high ϕ_A, while the light areas represent regions of low ϕ_A. The film surfaces are at the bottom and top of this figure, and there are periodic boundary conditions in the horizontal direction. The view in this plot is similar to that in Figure 1. The calculations are done for $\chi N = 20$, $N = 80$, and $f = 0.45$ on a 15×15 lattice.

addition, for slightly asymmetric diblock copolymers, a mixed perpendicular morphology, in which half of the film resembles the perpendicular morphology and the other half resembles a parallel morphology, becomes stable.

In the experiments of Morkved and Jaeger,[10,11] polystyrene−PMMA diblock copolymers are spin-coated onto a silicon nitride substrate. The copolymers have $\chi N \approx 20$ and are 47% PMMA by volume. It is known experimentally that, at a temperature of 155 °C, the silicon nitride substrate strongly prefers PMMA over polystyrene, while the free surface moderately prefers polystyrene over PMMA. TEM images of L-thick parts of the thin film taken at tilt angles ranging from 0° to 60° suggest that the film has a mixed perpendicular morphology in which the perpendicular domains extend through at most half of the film thickness and the rest of the film has a parallel morphology. However, TEM images do not produce a detailed three-dimensional structure. To relate the experiments to our calculations, we denote PMMA as A and polystyrene as B, the silicon nitride substrate as the bottom surface, and the free surface as the top surface. Thus, $\Delta\chi_{\text{bottom}} = \chi_{\text{B/bottom}} - \chi_{\text{A/bottom}}$ is large and positive, and $\Delta\chi_{\text{top}} = \chi_{\text{B/top}} - \chi_{\text{A/top}}$ is moderate and negative. Using the theory of Witten et al.[57,58] to take into account the different statistical segment lengths of PMMA (A) and polystyrene (B), we estimate f, the volume fraction of A, to be effectively 0.46. Our calculations predict that for large $\Delta\chi_{\text{bottom}}$ and moderate, negative $\Delta\chi_{\text{top}}$, the mixed perpendicular morphology, as in Figure 8, can indeed be stable. In addition, the mixed perpendicular morphology from our calculations, shown in Figure 8, is similar to Morkved and Jaeger's hypothesized structure, shown in Figure 11 (reprinted from ref 10). Our calculations are also consistent with temperature dependence experiments, which make use of the weaker preferential segregation of polystyrene to the free surface (less negative $\Delta\chi_{\text{top}}$) at higher temperatures. In the experimental polystyrene−PMMA films, as the annealing temperature is increased (thus making $\Delta\chi_{\text{top}}$ less negative), the perpendicular morphology becomes unstable, giving way to the parallel morphologies. This agrees with the phase diagram shown in Figure 6. However, our calculations
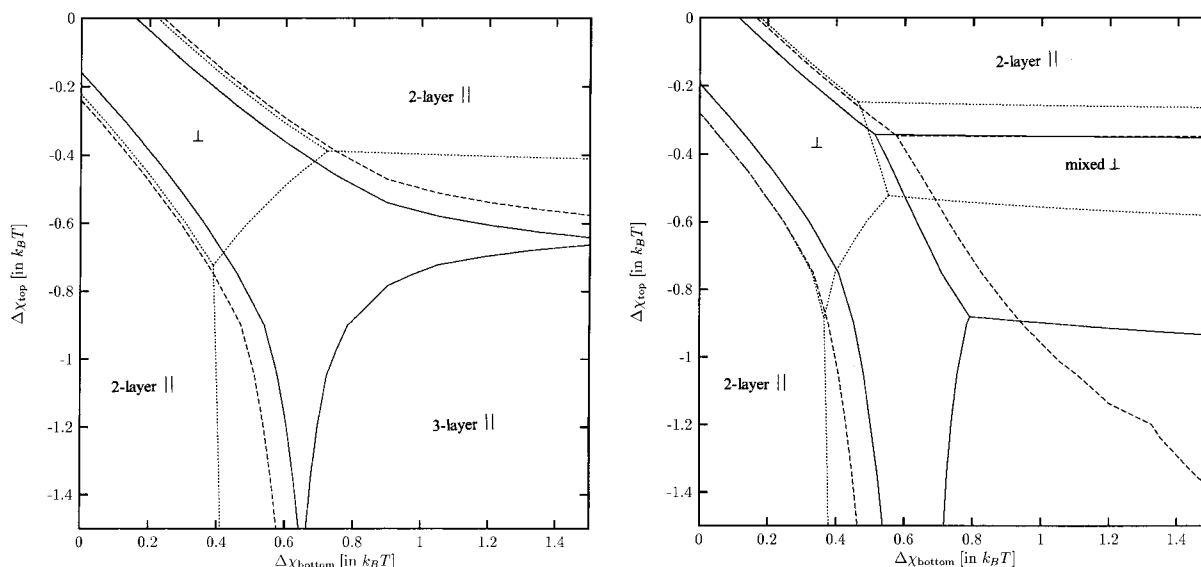
Figure 9. (a, left) Phase diagram showing the regions of stability for different morphologies for $\chi N = 20$, $N = 40$, $f = 0.5$, and film thicknesses of 10 (dashed lines), 11 (solid lines), and 12 (dotted lines) lattice sites. The two-layer parallel morphologies (as in Figure 1c,d) are stable in the upper right and lower left corners. The three-layer parallel morphology (as in Figure 1a) is stable in the lower right corner. The perpendicular morphology (as in Figures 1e or 5) is stable in the remaining region: $\Delta\chi_{bottom} \approx -\Delta\chi_{top}$ for small $|\Delta\chi_{bottom}|$ and $|\Delta\chi_{top}|$, $\Delta\chi_{top} \approx -0.6$ and large $\Delta\chi_{bottom}$ (film thickness of 10 or 11), and $\Delta\chi_{bottom} \approx 0.6$ and large, negative $\Delta\chi_{top}$ (film thickness of 10 or 11). Note that the boundary line between the regions of stability for the perpendicular morphology and the three-layer parallel morphology for a film thickness of 10 is off the scale of this diagram. (b, right) Phase diagram showing the regions of stability for different morphologies for $\chi N = 20$, $N = 40$, $f = 0.45$, and film thicknesses of 10 (dashed lines), 11 (solid lines), and 12 (dotted lines) lattice sites. The two-layer parallel morphologies (as in Figure 1c,d) are stable in the upper right and lower left corners. The three-layer parallel morphology (as in Figure 1a) is stable in the lower right corner. The perpendicular morphology (as in Figures 1e or 5) is stable for $\Delta\chi_{bottom} \approx -\Delta\chi_{top}$ for small $|\Delta\chi_{bottom}|$ and $|\Delta\chi_{top}|$, and $\Delta\chi_{bottom} \approx 0.5$ and large, negative $\Delta\chi_{top}$. The mixed perpendicular morphology (as in Figure 8) is stable for $\Delta\chi_{top} \approx -0.5$ and large $\Delta\chi_{bottom}$. Note that the boundary line between the regions of stability for the perpendicular or mixed perpendicular morphology and the three-layer parallel morphology for a film thickness of 10 is off the scale of this diagram.
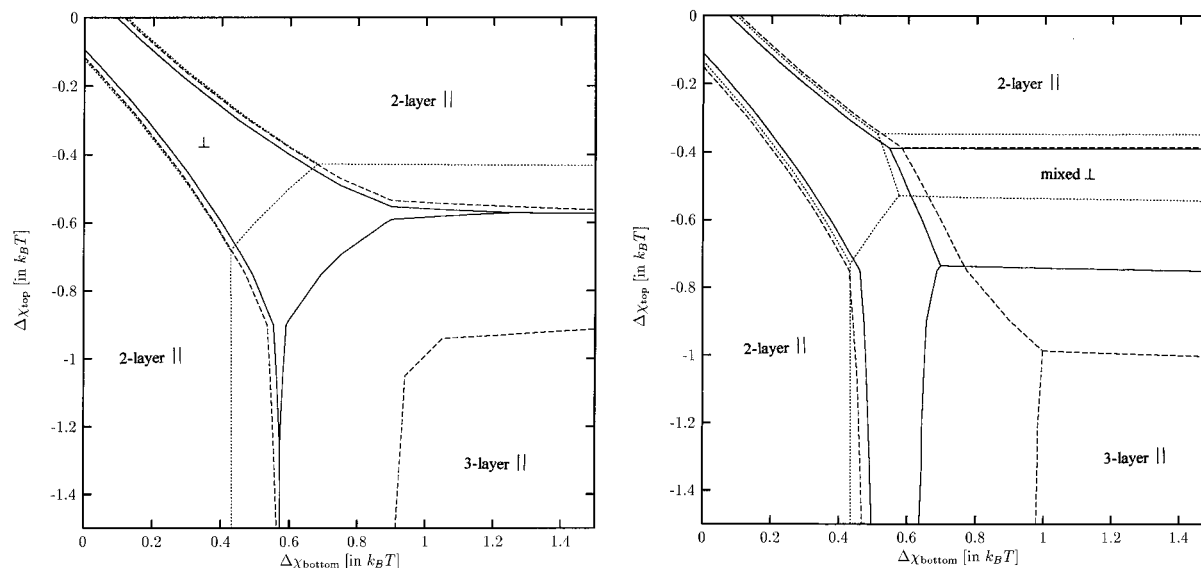

Figure 10. (a, left) Phase diagram showing the regions of stability for different morphologies for $\chi N = 30$, $N = 80$, $f = 0.50$, and film thicknesses of 16 (dashed lines), 17 (solid lines), and 18 (dotted lines) lattice sites. The two-layer parallel morphologies (as in Figure 1c,d) are stable in the upper right and lower left corners. The three-layer parallel morphology (as in Figure 1a) is stable in the lower right corner. The perpendicular morphology (as in Figures 1e or 5) is stable in the remaining region: $\Delta\chi_{bottom} \approx -\Delta\chi_{top}$ for small $|\Delta\chi_{bottom}|$ and $|\Delta\chi_{top}|$, $\Delta\chi_{top} \approx -0.5$ and large $\Delta\chi_{bottom}$ (film thickness of 16 or 17), and $\Delta\chi_{bottom} \approx 0.5$ and large, negative $\Delta\chi_{top}$ (film thickness of 16 or 17). (b, right) Phase diagram showing the regions of stability for different morphologies for $\chi N = 30$, $N = 80$, $f = 0.45$, and film thicknesses of 16 (dashed lines), 17 (solid lines), and 18 (dotted lines) lattice sites. The two-layer parallel morphologies (as in Figure 1c,d) are stable in the upper right and lower left corners. The three-layer parallel morphology (as in Figure 1a) is stable in the lower right corner. The perpendicular morphology (as in Figures 1e or 5) is stable for $\Delta\chi_{bottom} \approx -\Delta\chi_{top}$ for small $|\Delta\chi_{bottom}|$ and $|\Delta\chi_{top}|$, and $\Delta\chi_{bottom} \approx 0.5$ and large, negative $\Delta\chi_{top}$. The mixed perpendicular morphology (as in Figure 8) is stable for $\Delta\chi_{top} \approx -0.5$ and large $\Delta\chi_{bottom}$.

cannot explain the experimental observation that, under certain conditions, the films show a strong tendency to form L-thick films. Films originally cast with thickness slightly larger than L will, upon annealing at 155 °C, separate into regions of thickness L and regions of thickness $^3/_2L$. Purely thermodynamic considerations
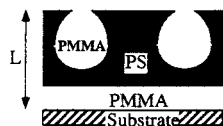
Figure 11. Hypothesized structure in Morkved and Jaeger's experiments on *L*-thick films of (approximately) symmetric polystyrene−PMMA diblock copolymers. Reprinted with permission from ref 10. Copyright 1997 Editions de Physique.

predict that the films should form regions of thicknesses $^1/_2L$ and $^3/_2L$; these are the thicknesses where the films are not frustrated. We can only suggest that the *L*-thick films are stable for kinetic reasons. The existence of metastable *L*-thick films has been observed experimentally in a similar system by Maaloum et al.[59]

In the experiments of Koneripalli et al.,[12] poly-(styrene-d_8)−poly(2-vinylpyridine) diblock copolymers ($\chi N \approx 20$) are confined between silicon or mica on one side and a glassy homopolymer on the other side. Poly-(2-vinylpyridine) segregates to the silicon or mica surface, while poly(styrene-d_8) segregates to the homopolymer interface. Neutron reflectivity measurements together with TEM images suggest that films of thickness *L* have a mixed perpendicular morphology, similar to the structure shown in Figure 8. However, we do not know the magnitudes of $\Delta\chi_{bottom}$ or $\Delta\chi_{top}$ (only the sign), and it is not clear to what degree the diblock copolymers might be asymmetric.

The predictions of our calculations are amenable to direct experimental verification. The surface energies of the confining walls can be controlled by using end-grafted random copolymer brushes of variable composition.[60] Low-voltage, high-resolution scanning electron microscopy together with reactive ion etching can produce three-dimensional images of copolymer thin films with reasonable resolution.[61] A combination of these experimental techniques would allow a systematic study of the effect of preferential surface energies on diblock copolymer thin film morphology, similar to the calculations presented here.

We note that, for the type of diblock copolymer films studied in this paper (asymmetric surface conditions, so that one species (A) is preferred at the bottom surface and the other species (B) is preferred at the top surface), *L*-thick films are frustrated, but *L* is not the thickness of maximum frustration. In *L*-thick films with the one-layer parallel morphology, the chains are stretched by a factor of 2, while in *L*-thick films with the three-layer parallel morphology, the chains are compressed by a factor of $^2/_3$. In the strong segregation limit, the one-layer parallel morphology has free energy (neglecting surface energy) $^5/_3F_0$, where F_0 is the free energy of the bulk diblock copolymer, and the three-layer parallel morphology has free energy $^{31}/_{27}F_0$. The thickness of maximum frustration, as measured by the difference in free energy between the stretched or compressed film and the bulk diblock copolymer, is $^3\sqrt{9/_{16}}L \approx 0.825L$. We expect that the perpendicular morphology would be most stable when the film is maximally frustrated. Thus, it is not surprising that, for films of thickness close to *L*, decreasing the thickness increases the region of stability for the perpendicular morphology, as illustrated in Figures 6, 7, 9, and 10.[62]

It would be interesting to perform some Scheutjens−Fleer calculations for larger two-dimensional lattices or three-dimensional lattices. One might expect three-dimensional calculations on thin films to exhibit even

richer behavior than two-dimensional calculations. However, the computation time increases very rapidly as the number of lattice sites increases. Consequently, doing Scheutjens−Fleer calculations for larger two-dimensional lattices or any three-dimensional lattice would require either much faster computers or better techniques for numerically solving the Scheutjens−Fleer equations.

V. Conclusions

We performed a systematic study of the role of preferential surface energies in confined diblock copolymer thin films. Our Scheutjens−Fleer calculations focused on symmetric and nearly symmetric diblock copolymers of thickness *L* and predicted a much richer phase behavior than that predicted by the simple, strong segregation limit, flat interface theory. While the simple, strong segregation limit, flat interface theory essentially predicts that only the parallel morphologies are stable, the Scheutjens−Fleer calculations predict the existence of perpendicular and mixed perpendicular morphologies for certain values of $\Delta\chi_{bottom}$ and $\Delta\chi_{top}$. These perpendicular and mixed perpendicular morphologies are those in which some part of the A−B interface is perpendicular to the film surfaces. Such perpendicular phases are of special interest for surface patterning applications. In addition to the nearly-flat interface perpendicular morphology expected near neutral wetting conditions, the calculations predict a new morphology in which one species wets the bottom surface while the top surface has alternating A and B stripes. The Scheutjens−Fleer calculations are also consistent with the experimental observation of the mixed perpendicular morphology in *L*-thick films,[10−12] but we cannot make a detailed comparison because many of the experimental parameters are unknown. Moreover, we do not establish a quantitative correspondence between our numerical parameters, such as *N*, $\Delta\chi_{bottom}$, and $\Delta\chi_{top}$, and physical quantities, such as molecular weight and surface energies. However, if one could identify a correspondence between some feature on our calculated phase diagrams and experimental results, one could then make detailed quantitative comparisons between our calculations and experiment. It should also be noted that there is no guarantee that all the possible morphologies have been discovered. As discussed in section II, the solutions we obtained depend on the initial conditions supplied.

Our calculations find *two* distinct perpendicular morphologies—the usual perpendicular morphology and a novel mixed perpendicular morphology not considered in previous studies of diblock copolymer thin films. This new mixed perpendicular morphology is found only when the diblock copolymers are slightly asymmetric. Previous theoretical studies often consider perfectly symmetric diblock copolymers only, but the "symmetric" diblock copolymers used in experiments are rarely perfectly symmetric. Our calculations also predict the region of stability for the new mixed perpendicular morphology in terms of $\Delta\chi_0$, the amount of preferential wetting needed on both film surfaces to make the two-layer parallel morphology and the three-layer parallel morphology equal in free energy. (In the strong segregation limit, $\Delta\chi_0$ corresponds to a surface energy equal to $^4/_9$ times the A−B interfacial energy.[17]) For slightly asymmetric diblock copolymers, similar to those of refs 10 and 11, the mixed perpendicular morphology is stable when the wetting preference of one surface for the

minority species exceeds $\Delta\chi_0$ (approximately) and the other surface prefers the majority species with an energy of roughly $\Delta\chi_0$.

Our calculations consider thin films with flat surfaces. However, there is no reason why the surfaces of free-surface thin films must be perfectly flat. In fact, AFM studies suggest that the free-surface thin films in the experiments of Morkved and Jaeger are rippled.[11] Several theoretical studies have investigated rippling in diblock copolymer thin films with parallel morphologies and find that rippled surfaces are generally energetically unfavorable compared to flat surfaces,[63-65] However, the spontaneous rippling observed experimentally by Morkved and Jaeger suggests that the mixed perpendicular morphology in diblock copolymer thin films with rippled surfaces is *lower* in free energy than the mixed perpendicular morphology with flat surfaces. This spontaneous rippling should also stabilize the mixed perpendicular morphology in comparison to the parallel morphologies. It would be interesting to do a detailed study of the effect of rippling in the different thin film morphologies.

Our calculations give no hint as to why the physical films studied in refs 10 and 11 seem to select a thickness near *L*. We could see no reason for such selection on the basis of the thickness dependence of the equilibrium free energies. The origin of this selection remains an important question for future work to address.

References and Notes

(1) Bates, F. S.; Fredrickson, G. H. *Annu. Rev. Phys. Chem.* **1990**, *41*, 525.
(2) Binder, K. *Adv. Polym. Sci.* **1994**, *112*, 181.
(3) It is possible (though not easy) to obtain neutral wetting. See: Mansky, P.; Liu, Y.; Huang, E.; Russell, T. P. *Science* **1997**, *275*, 1458. Mansky, P.; et al. *Phys. Rev. Lett.* **1997**, *79*, 237.
(4) Coulon, G.; Russell, T. P.; Deline, V. R.; Green, P. F. *Macromolecules* **1989**, *22*, 2581.
(5) Anastasiadis, S. H.; Russell, T. P.; Satija, S. K.; Majkrzak, C. F. *J. Chem. Phys.* **1990**, *92*, 5677.
(6) Coulon, G.; Ausserre, D.; Russell, T. P. *J. Phys. (Paris)* **1990**, *51*, 777.
(7) Coulon, G.; Collin, B.; Ausserre, D.; Chatenay, D.; Russell, T. P. *J. Phys. (Paris)* **1990**, *51*, 2801.
(8) Carvalho, B. L.; Thomas, E. L. *Phys. Rev. Lett.* **1994**, *73*, 3321.
(9) Henkee, C. S.; Thomas, E. L.; Fetters, L. J. *J. Mater. Sci.* **1988**, *23*, 1685.
(10) Morkved, T. L.; Jaeger, H. M. *Europhys. Lett.* **1997**, *40*, 643.
(11) Morkved, T. L. *Experimental Studies of Morphology and of Its Control in Diblock Copolymer Ultrathin Films*. Ph.D. thesis, University of Chicago, 1997.
(12) Koneripalli, N.; Levicky, R.; Bates, F. S.; Ankner, J.; Kaiser, H.; Satija, S. K. *Langmuir* **1996**, *12*, 6681.
(13) Kellogg, G. J.; Walton, D. G.; Mayes, A. M.; Lambooy, P.; Russell, T. P.; Gallagher, P. D.; Satija, S. K. *Phys. Rev. Lett.* **1996**, *76*, 2503.
(14) Hasegawa, H.; Hashimoto, T. *Polymer* **1992**, *33*, 475.
(15) Schwark, D. W.; Vezie, D. L.; Reffner, J. R.; Thomas, E. L.; Annis, B. K. *J. Mater. Sci. Lett.* **1992**, *11*, 352.
(16) Vezie, D. L.; Thomas, E. L.; Adams, W. W. *Polymer* **1995**, *36*, 1761.
(17) Turner, M. S. *Phys. Rev. Lett.* **1992**, *69*, 1788.
(18) Walton, D. G.; Kellogg, G. J.; Mayes, A. M.; Lambooy, P.; Russell, T. P. *Macromolecules* **1994**, *27*, 6225.
(19) Kikuchi, M.; Binder, K. *J. Chem. Phys.* **1994**, *101*, 3367.
(20) Pickett, G. T.; Balazs, A. C. *Macromolecules* **1997**, *30*, 3097.
(21) Sommer, J.-U.; Hoffmann, A.; Blumen, A. *J. Chem. Phys.* **1999**, *111*, 3728.
(22) Matsen, M. W. *J. Chem. Phys.* **1997**, *106*, 7781.
(23) Brown, G.; Chakrabarti, A. *J. Chem. Phys.* **1995**, *102*, 1440.
(24) Pickett, G. T.; Witten, T. A.; Nagel, S. R. *Macromolecules* **1993**, *26*, 3194.
(25) Mansky, P.; Chaikin, P.; Thomas, E. L. *J. Mater. Sci.* **1995**, *30*, 1987.
(26) Zehner, R. W.; Lopes, W. A.; Morkved, T. L.; Jaeger, H.; Sita, L. R. *Langmuir* **1998**, *14*, 241.
(27) Helfand, E. *Acc. Chem. Res.* **1975**, *8*, 295.
(28) Helfand, E.; Wasserman, Z. R. *Polym. Eng. Sci.* **1977**, *17*, 582.
(29) Matsen, M. W.; Schick, M. *Phys. Rev. Lett.* **1994**, *72*, 2660.
(30) Matsen, M. W.; Bates, F. S. *Macromolecules* **1996**, *29*, 1091.
(31) Hong, K. M.; Noolandi, J. *Macromolecules* **1981**, *14*, 727.
(32) Whitmore, M. D.; Noolandi, J. *J. Chem. Phys.* **1990**, *93*, 2946.
(33) Whitmore, M. D.; Vavasour, J. D. *Acta Polym.* **1995**, *46*, 341.
(34) Shull, K. R.; Kramer, E. J. *Macromolecules* **1990**, *23*, 4769.
(35) Shull, K. R. *Macromolecules* **1992**, *25*, 2122.
(36) Ben-Shaul, A.; Szleifer, I.; Gelbart, W. M. *J. Chem. Phys.* **1985**, *83*, 3597.
(37) Carignano, M. A.; Szleifer, I. *J. Chem. Phys.* **1993**, *98*, 5006.
(38) Fleer, G. J.; Stuart, M. A. C.; Scheutjens, J. M. H. M.; Cosgrove, T.; Vincent, B. *Polymers at Interfaces*; Chapman & Hall: London, 1993.
(39) Evers, O. A.; Scheutjens, J. M. H. M.; Fleer, G. J. *Macromolecules* **1990**, *23*, 5221.
(40) Scheutjens, J. M. H. M.; Fleer, G. J. *J. Phys. Chem.* **1979**, *83*, 1619.
(41) Huang, K.; Balazs, A. C. *Phys. Rev. Lett.* **1991**, *66*, 620.
(42) Huang, K.; Balazs, A. C. *Macromolecules* **1993**, *26*, 4736.
(43) Atkins, P. W. *Physical Chemistry*; W. H. Freeman and Co.: New York, 1990.
(44) Freed, K. F.; Bawendi, M. G. *J. Phys. Chem.* **1989**, *93*, 2194.
(45) de Gennes, P.-G. *Scaling Concepts in Polymer Physics*; Cornell University Press, Ithaca, 1979.
(46) Flory, P. J. *Statistical Mechanics of Chain Molecules*; Interscience Publishers: New York, 1969.
(47) Equations 3−9 are definitions for convenience. For each of the $m_x m_z$ lattice sites, there are essentially three equations: eqs 10 and 11, which make use of these definitions, together with the constraint eq 2. Given arbitrary ϕ_A, ϕ_B, and u' fields, eqs 10 and 11 give new values of $\tilde{\phi}_A(\phi_A, \phi_B, u')$ and $\tilde{\phi}_B(\phi_A, \phi_B, u')$. The correct fields are those that satisfy $\tilde{\phi}_A(\phi_A, \phi_B, u') = \phi_A$, $\tilde{\phi}_B(\phi_A, \phi_B, u') = \phi_B$, and $\phi_A + \phi_B = 1$ at every point (x, z).
(48) Rabinowitz, P., Ed. *Numerical Methods for Nonlinear Algebraic Equations*; Gordon and Breach Science Publishers: London, 1970.
(49) More, J. J.; Garbow, B. S.; Hillstrom, K. E. User guide for MINPACK-1. Technical Report ANL-80-74, Argonne National Laboratory, Argonne, IL, 1980.
(50) A detailed derivation of this result can be found in refs 38 and 39.
(51) Leibler, L. *Macromolecules* **1980**, *13*, 1602.
(52) The computer code implementing the Scheutjens−Fleer method is available at http://ars-www.uchicago.edu/~wtang/sf/sf.html.
(53) Lin, Y.-H. *Macromolecules* **1987**, *20*, 3080.
(54) Russell, T. P.; Hjelm, R. P.; Seeger, P. A. *Macromolecules* **1990**, *23*, 890.
(55) Since free energies are computed at only a discrete set of $\Delta\chi_{bottom}$ and $\Delta\chi_{top}$ values, the phase boundaries shown are obtained by linear interpolation.
(56) Pickett, G. T. Private communication.
(57) Witten, T. A.; Milner, S. T.; Wang, Z.-G. Theory of stress distribution in block copolymer microdomains. In *Multiphase Macromolecular Systems*; Culbertson, B. M., Ed.; Plenum Press: New York, 1989.
(58) Unless the two blocks of a diblock copolymer are completely symmetric, the diblock copolymer bilayer will tend to have some curvature. Reference 57 estimates the free energy of a slightly asymmetric diblock copolymer bilayer to be

$$F \approx \frac{\pi^2}{24}\sigma^2 a_E V_E \left[1 - \frac{3}{2}\frac{\sigma V_E}{R} + \frac{13}{5}\left(\frac{\sigma V_E}{R}\right)^2 \right] + \frac{\pi^2}{24}\sigma^2 a_I V_I \left[1 + \frac{3}{2}\frac{\sigma V_I}{R} + \frac{13}{5}\left(\frac{\sigma V_I}{R}\right)^2 \right] + \frac{\gamma}{\sigma}$$

where σ is the number of chains per unit area, R is the radius of curvature of the bilayer, a_E is the "packing length" for the block on the exterior of the curved bilayer, V_E is the volume displaced by the exterior block, a_I is the packing length for

the block on the interior of the curved bilayer, V_I is the volume displaced by the interior block, and γ is the interfacial energy per unit area. The packing length is related to chain flexibility and is given by

$$a = \frac{m_0}{\rho} \frac{3}{C_\infty b^2}$$

where m_0 is the molecular weight per backbone bond, ρ is the density (mass per unit volume), b is the backbone bond length, and C_∞ is the characteristic ratio. At equilibrium, the bilayer adopts the σ and $1/R$ that minimize the free energy F. In the experimental system of Morkved and Jaeger, $V_{polystyrene} = V_E = 0.53 V$ (where V is the total volume displaced by the entire diblock copolymer chain), $V_{PMMA} = V_I = 0.47 V$, $a_{polystyrene} = a_E = 11.5$ Å, and $a_{PMMA} = 10.6$ Å. The equilibrium $1/R$ is calculated ($\partial F/\partial \sigma = 0$, $\partial F/\partial(1/R) = 0$) to be $0.0877(a_{polystyrene}/(\gamma V^2))^{1/3}$. For a diblock copolymer with blocks of identical flexibility ($a_E = a_I$), as in our Scheutjens−Fleer calculations, to attain an equilibrium curvature of $1/R = 0.0877(a_{polystyrene}/(\gamma V^2))^{1/3}$, V_I must be $0.46 V$.

(59) Maaloum, M.; Ausserre, D.; Chatenay, D.; Gallot, Y. *Phys. Rev. Lett.* **1993**, *70*, 2577.

(60) Mansky, P.; Liu, Y.; Huang, E.; Russell, T. P. *Science* **1997**, *275*, 1458.

(61) Harrison, C.; Park, M.; Chaikin, P. M.; Register, R. A.; Adamson, D. H.; Yao, N. *Polymer* **1998**, *39*, 2733.

(62) The observant reader might note that while the strong segregation limit, flat interface theory predicts that the perpendicular morphology is stable in a region of zero area in the $\Delta\chi_{bottom} - \Delta\chi_{top}$ plane when the film thickness is exactly L (see the Introduction), the simple theory also predicts that the perpendicular morphology is stable in a small but nonzero area in the $\Delta\chi_{bottom} - \Delta\chi_{top}$ plane when the film thickness is close to but not equal to L. Nevertheless, the phase diagrams obtained from Scheutjens−Fleer calculations exhibits richer behavior (compared to that predicted by the simple theory), such as an expanded region of stability for the perpendicular morphology and the existence of a novel mixed perpendicular morphology.

(63) Turner, M. S.; Joanny, J.-F. *Macromolecules* **1992**, *25*, 6681.

(64) Fredrickson, G. H.; Ajdari, A.; Leibler, L.; Carton, J.-P. *Macromolecules* **1992**, *25*, 2882.

(65) Xi, H.-W.; Milner, S. T. *Macromolecules* **1996**, *29*, 4772.